# Structural Molecular Dynamics Studies on Polyamidoamine Dendrimers for a Therapeutic Application: Effects of pH and Generation

**Inhan Lee,[†] Brian D. Athey,[‡] Arthur W. Wetzel,[§] Walter Meixner,[‡] and James R. Baker, Jr.*,[†]**

*Department of Internal Medicine and Center for Biologic Nanotechnology and Department of Cell & Development Biology, University of Michigan, Ann Arbor, Michigan 48109, and Pittsburgh Supercomputing Center (PSC), Carnegie Mellon University, Pittsburgh, Pennsylvania 15213*

ABSTRACT: Extensive simulations of PAMAM dendrimer generation 2 were performed at several pH conditions with explicit water molecules, to obtain proper conditions and validity for additional simulations without explicit water. Within the range of validity, simulation without water greatly extends the size and duration of practical simulations. We investigated the effects of long-range interaction parameters such as interaction distance and dielectric constant for molecular dynamics simulations of PAMAM dendrimer without water, concluding that charged dendrimer simulation with distance-dependent dielectric constant but without cutoff distance best mimics explicit water results. Structural variations of PAMAM dendrimers were analyzed as a function of pH and dendrimer generation using MD simulations with these long-range interaction parameters. Globular and loosely compact structures at high pH ($\geq 10$) show conservation of atom density distribution across dendrimer generations. Highly ordered extended structures at low pH ($\leq 4$) present an increasingly hollow interior as dendrimer generation grows, resulting in more open structure which provides easier access by chemical agents. By contrast, significant branch back-folding occurred at neutral pH in addition to major peripheral distribution of the terminal groups, yielding higher interior density in the intermediate radial region between the center and the maximum radius as the generation grows. Higher generation dendrimers provide a cavity surrounded by dense atom populations, producing a more stable agent carrier. Transition to high-density packing occurs between generations 4 and 5. Volume differences between neutral and low pH calculated from $R_G$ show a dramatic increase beginning at generation 5.

## Introduction

Synthetic polymers have many uses in biomedical applications, based on their ease of manufacture, durability, and low immunogenicity.[1] Polyamidoamine (PAMAM) dendrimers are the only polymers with unidispersed and well-defined molecular structures. These molecules can be synthesized in large quantities and have a large number of potential biomedical applications. Several groups, including our own, have successfully used PAMAM dendrimers as a gene delivery system,[2-4] and we are now developing them as delivery systems for other therapeutic agents. Other groups have found PAMAM dendrimers suited to drug delivery systems.[5,6]

Desired features of effective drug delivery include (1) protection of agents, (2) targeting to specific tissues, cells, and cellular compartments, and (3) release of agents in the target area either continuously at a proper rate or in response to external signals. There are several paths of uptake of exogeneous materials into a cell with endocytosis being the most efficient pathway for the uptake of macromolecules.[7] Consequently, escape from the endosome is critical for the cytosolic delivery of any macromolecule before it is degraded in the lysosome. One major feature of the endosome is its local pH of ~5, while the cytosolic pH is ~7.4. At physiological pH 7.4.

most primary amines of the PAMAM dendrimer are protonated, while tertiary amines inside the dendrimer are not protonated until the pH drops to 4.[8] It is speculated that changes in pH structurally alter PAMAM dendrimers, leading to endosomal disruption.

Computer simulations are widely used in polymer science. Dendrimers have been investigated using various theoretical models and computer simulations such as self-consistent-field calculations,[9] Monte Carlo (MC) simulations,[10,11] and molecular dynamics (MD) simulations.[12,13] In contrast to MC simulation, MD simulations can yield dynamic information. There are two general types of MD simulations: coarse-grain and atomistic. Coarse-grain MD simulations can give information about a large system within a reasonable computational time frame, while atomistic MD simulation offers specific molecular information but requires considerably more computational time.

While coarse-grain MD studies on dendrimers[13] were used to predict general properties, atomistic MD simulations on dendrimers were performed to provide 3D structures of specific dendrimers[14-16] and to suggest possible interactions in dendrimer formation.[17] Recently, more exhaustive atomistic MD simulations on dendrimers were carried out to study their solution behavior,[18] potential use as catalyst supports,[19] the effect of repeat unit flexibility,[20] and several nanoscale applications.[21] Dendritic polyelectrolytes have been modeled using MC simulations,[22] and several pH-dependent dendrimer experiments have been performed.[23,24] However, none of these simulations have dealt with pH-dependent protonated dendrimer, which is important to biological study and applications.

[†] Department of Internal Medicine and Center for Biologic Nanotechnology, University of Michigan.
[‡] Department of Cell & Development Biology, University of Michigan.
[§] Carnegie Mellon University.
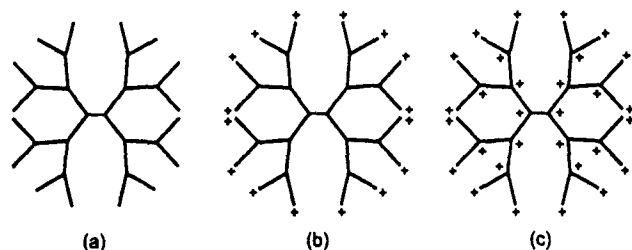* Corresponding author: e-mail jbakerjr@umich.edu; Fax 734-936-9220; phone 734-647-2777.

**Figure 1.** Schematic diagram of generation-2 dendrimer at (a) high pH, (b) neutral pH, and (c) low pH.

Protonation processes at different pH, a part of biological events, occur in aqueous solution. However, an atomistic MD simulation with explicit water is very expensive in both computation time and memory and can rapidly exceed the capacity of current software and hardware. Simulation without explicit water, on the other hand, yields uncertain results. There are methods to mimic a water environment such as the Poisson–Boltzmann method,[25] which also has limitations on model size and takes several times longer than simulation in vacuum conditions.

In this study, we used atomistic MD simulations to study PAMAM dendrimers produced from an ethylenediamine (EDA) core in a variety of simulated physicochemical conditions such as pH and dendrimer generation. Since simulations with water molecules are very expensive, we investigated parameters for simulations without explicit water to optimize a range of operation which still adequately mimics the essential characteristics of water effects. Extensive MD simulations of small dendrimers (generation 2) were performed with explicit water molecules at different pH conditions. These simulations were compared to simulations without water while changing several simulation parameters. After choosing an optimal parameter set for simulations without water molecules, we studied pH effects on PAMAM dendrimer structures as a function of dendrimer generation under these optimized conditions. Structural variance corresponding to dendrimer generation was investigated by calculating the radial atom density of the dendrimer from the center of mass as well as the terminal nitrogen atom density at various pH conditions. In addition, the structural changes of dendrimers of different generations in low ($\leq$4) and neutral pH was of great interest because of pH changes naturally occurring in the compartments of living cells.

## Simulation Conditions

Based on pH titration data, three simulation conditions were designed to represent the effect of pH: no amines are assumed to be protonated above pH 10, all primary amines are protonated at pH 7, and all amines of a dendrimer are protonated below pH 4. We will refer to these conditions as high pH, neutral pH, and low pH, respectively (Figure 1). Molecular models of PAMAM dendrimers (EDA core) from generations 2 to 6 were built for these pH values on an Onyx workstation (Silicon Graphics, Inc., Mountain View, CA) using the Insight II software package (Accelrys Inc., San Diego, CA). The physical properties of the model dendrimers are shown in Table 1.

Since our models contain strong charges, such as those found in aqueous solutions, it is necessary to determine the validity of simulation without explicit water molecules. This was tested using dendrimers of generation 2 with a 10 Å water layer on each of the

**Table 1. Physical Properties of EDA Core PAMAM Dendrimer Models**

| generation | pH[a] | no. of atoms | mol wt | total charge |
|---|---|---|---|---|
| 2 | low | 546 | 3286.5 | 30 |
| | neutral | 532 | 3272.4 | 16 |
| | high | 516 | 3256.3 | 0 |
| 3 | low | 1154 | 6971.5 | 62 |
| | neutral | 1124 | 6941.3 | 32 |
| | high | 1092 | 6909.0 | 0 |
| 4 | low | 2370 | 14341.6 | 126 |
| | neutral | 2308 | 14279.1 | 64 |
| | high | 2244 | 14214.6 | 0 |
| 5 | low | 4802 | 29081.7 | 254 |
| | neutral | 4676 | 28954.7 | 128 |
| | high | 4548 | 28825.7 | 0 |
| 6 | low | 9666 | 58561.9 | 510 |
| | neutral | 9412 | 58305.8 | 256 |
| | high | 9156 | 58047.8 | 0 |

[a] Low and high pH refers to lower than pH 4 and higher than pH 10, respectively. Amine protonation depends on the dendrimer generation from our pH titration study (data not shown).

dendrimers over the pH range to ensure the hydrogen bond interaction range was covered. After the steepest descent minimization process for 5000 steps, the initial configuration was set as number one. MD simulations were performed either on an Onyx using a consistent valence force field (CVFF)[26] of Insight II or on a Compaq Alphaserver cluster with 64 4-processor nodes using CHARMM[27] software. All atoms were included in the potential energy calculations. After the simulation continued for 200 ps at 295 K (room temperature) with 1 fs intervals from the initial configuration number one (ICN1), the temperature of the model system was increased to 1000 K and equilibrated for 11 ps at that temperature. Among the configurations of the 1000 K simulation, we select one and minimize its energy for 5000 steps to prepare another initial configuration number two (ICN2). Total simulation times of dendrimers from each initial configuration were 400 ps at neutral and low pH and 1.5 or 1.8 ns at high pH. Final configurations from ICN1 and ICN2 were compared to confirm equilibrium. The average or both of the two configurations were used for comparison to results from simulations without explicit water molecules.

The total potential energy function for MD calculations is described as

$$U_{\text{total}} = U_{\text{bonded}} + U_{\text{nonbonded}}$$

$$U_{\text{nonbonded}} = U_{\text{Lennard-Jones}} + U_{\text{Coulomb}}$$

$$= \frac{1}{2}\sum_i\sum_j\left\{\epsilon\left[\left(\frac{\sigma}{r}\right)^{12} - 2\left(\frac{\sigma}{r}\right)^6\right] + \frac{q_i q_j}{Dr}\right\} \quad (1)$$

where $\epsilon$ is the minimum energy of Lennard-Jones potential, $\sigma$ is the distance to give minimum Lennard-Jones potential, $q$ is the partial charge on the atom, $D$ is the dielectric constant (1 for vacuum), $r$ is the distance between $i$ and $j$, and $i$, $j$ are nonbonded atom pairs. Interactions between nonbonded atoms are usually short range if the Coulomb energy term is not dominant in the above equation. Therefore, most MD simulations calculate potential energies between particles only within a limited nonbond cutoff distance ($r_c$). However, since our models at low and neutral pH contain many positive charges, and the long-range Coulomb energy is dominant, we need to consider the effect of long-range interactions.
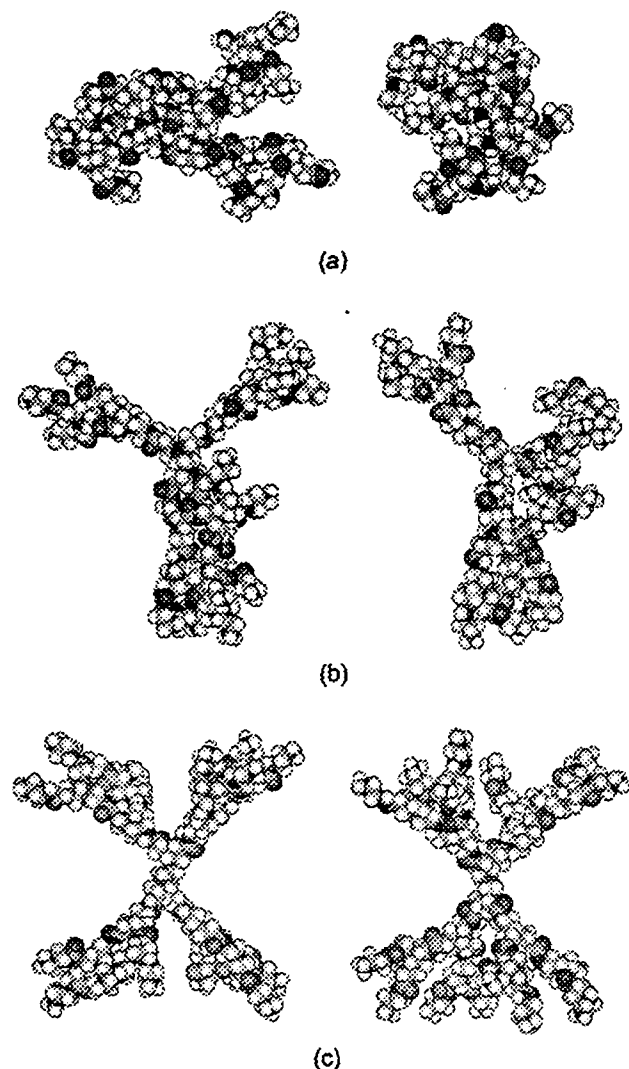
**(a)**



**(b)**



**(c)**

**Figure 2.** Final simulated configurations at (a) high, (b) neutral, and (c) low pH, starting from the initial configuration number one (left) and number two (right). Water molecules, explicitly included in the actual simulation, are not shown.



**Figure 3.** Density profiles of G2 dendrimer with water molecules at high pH (a, b), neutral pH (c, d), and low pH (e, f). Left panels (a, c, e) show the atom densities, and right panels (b, d, f) show the densities of terminal nitrogen atoms. Blue plots are results from ICN1 and red from ICN2. These graphs correspond to Figure 2.

Simulations of generation 2 (G2) nonhydrated PAM-AM dendrimers were performed under the two combined conditions of nonbonded potential energy calculation: (1) potential energy calculation range (nonbond cutoff distance $r_c$) and (2) dielectric constant $D$ in the Coulomb energy. We either included all atoms in the energy calculation ($r_c = \infty$) or did not include potential energies between atoms farther than 11 Å apart ($r_c = 11$ Å). We also used the dielectric constant $D = 1$ (vacuum) or distance-dependent dielectric constant ($D = r$). After the steepest descent minimization for 1000 steps, each model was annealed for 5 ps at 1000 K. Then, the temperature was cooled to 295 K and simulation performed for 100 ps. All simulations were performed on an Onyx using Insight II software and on an Alphaserver cluster using CHARMM software to check software and hardware dependency.

On the basis of comparison between simulation results with and without water, we chose the long-range interaction conditions for nonhydrated PAMAM dendrimer simulations such as (1) $r_c = \infty$ and (2) $D = r$. Under these conditions, PAMAM dendrimers of generations 3–6 (EDA core) were simulated at different pH values on an Onyx using the CVFF force field of the Insight II software package. All simulations were
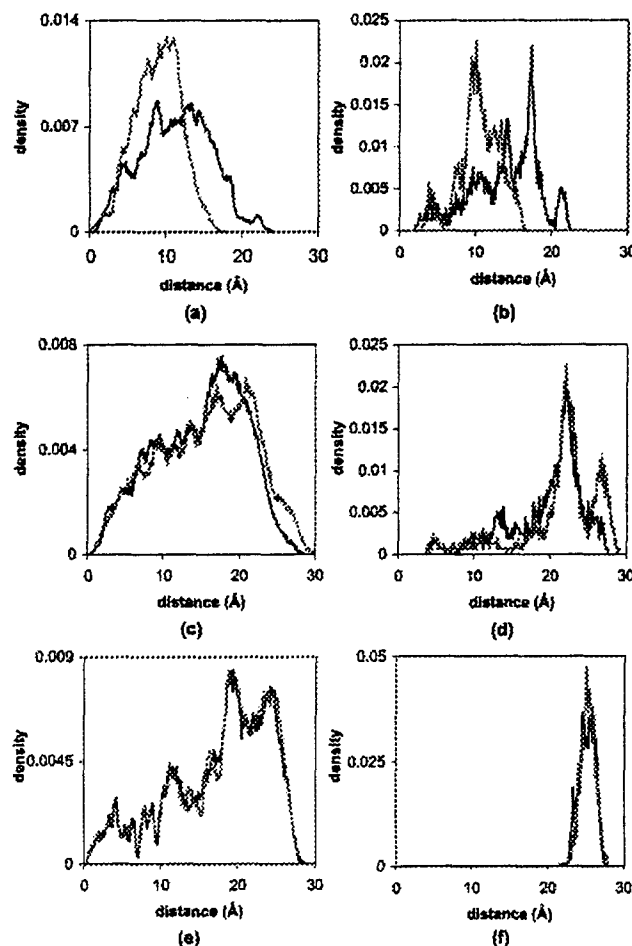
performed for 100 ps (at least twice the equilibration time) at 295 K with 1 fs intervals after energy minimization and system annealing processes as previously described. To ensure the equilibration, the larger generation 5 and 6 dendrimers were simulated using another initial configuration similar to the G2 models with water. All data used for evaluation were collected from the simulations after equilibration.

## Results and Discussion

The computation time of simulations with explicit water molecules is extremely expensive. The average service unit (SU: 1 SU = 1 h of CPU time) for 100 ps simulation of G2 PAMAM dendrimer with a 10 Å hydration layer at high pH and 1 fs time step (ts) was 170.24 (5.32 h with 32 processors) on a Compaq Alphaserver cluster with 667 MHz 21264A processors. The SU charge for the 100 ps simulation of G2 dendrimer without water under the same conditions ($D = 1$, $r_c = \infty$, ts = 1 fs) was 1.52 (0.38 h with four processors), which is the longest among nonhydrated models. Therefore, simulations with water are more than 100 times more expensive than nonhydrated simulations for dendrimer generation 2. This difference can even increase at higher generation levels limiting the current practically of explicit water simulations of dendrimers for biological applications. If we can predict a major feature from nonhydrated simulations with a proper parameter
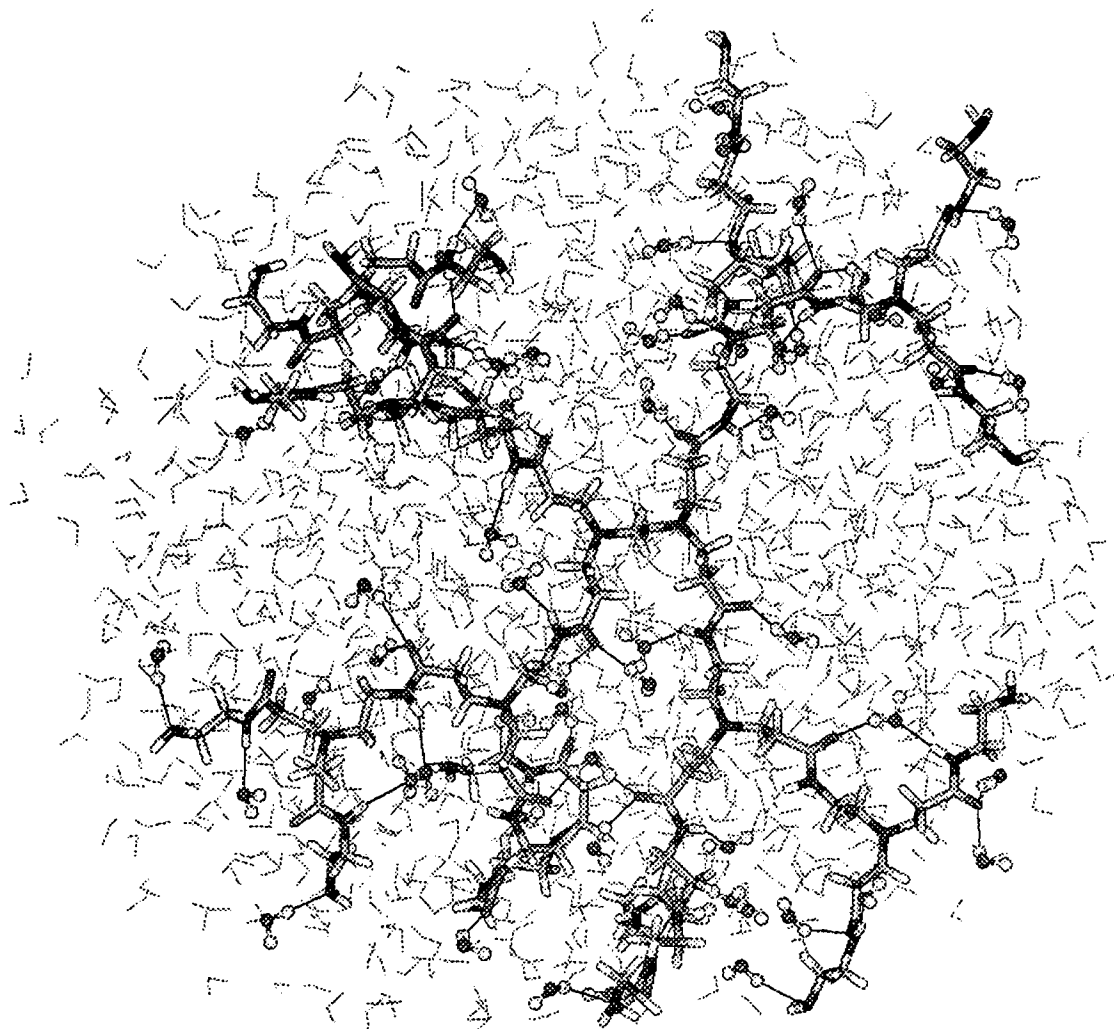
**Figure 4.** The G2 dendrimer configuration with water molecules after 200 ps simulation from ICN1 at high pH. The annealing process at 1000 K to generate ICN3 started from this configuration. Black lines represent hydrogen bonds between water molecules and the G2 dendrimer at high pH. These bonded water molecules are rendered as ball-and-stick, while all other water molecules are blue-lined.

choice, the simulation serves as a useful and practical tool. This helps to guide later investigation into more specific applications that may require explicit water simulation to capture specific details.

G2 PAMAM dendrimer molecules with a 10 Å hydration layer at each of the three pH conditions were simulated without nonbond cutoff in order to include all long-range charge interactions in the model. ICN1's at each of the pH conditions were very close to each other (homogeneous and extended). After the initial 200 ps simulation and consecutive annealing process, we could obtain very different ICN2's from ICN1's at different pH conditions. The final configurations after MD simulations for each pH are shown in Figure 2. comparing the cases of ICN1 and ICN2. The final configurations of neutral and low pH are after 400 ps simulation time. Their features show high similarity between two different initial configuration cases. The final configurations of high pH are after 1500 ps simulations yet still present somewhat different features depending on the initial configuration. Neutral- and low-pH dendrimer molecules reached equilibration much faster than high-pH molecules, probably due to extensive charge interactions. In the high-pH model there is little driving force to overcome the energy barrier between the two configurations in Figure 2a, where the net charge is zero.

We calculated the atom density of dendrimer ensembles collected from snapshots, after system equilibration was assumed. For each snapshot configuration we calculated the histogram of the distances of all atoms from the center of mass. All collected histograms of dendrimer ensembles were normalized by the total number of atoms (unless described separately). The density of terminal nitrogen atoms in amine groups was similarly calculated on the basis of radial distance of terminal nitrogen atoms from the center of mass normalized by total number of terminal nitrogen atoms (unless described separately).

Figure 3 shows the atom density and the density of terminal nitrogen atoms corresponding to Figure 2. Each graph consists of 500–1000 ensembles close to the final configuration. The final configurations at low pH give a very narrow atom distribution including the distribution of terminal nitrogen atoms localized in finite range (Figure 3e,f). There is a slight shift of density profiles at neutral pH (Figure 3c.d). However, the inner radial profiles of the atom density are very similar, and the major peak of terminal nitrogen density profile of each model is found at the same place. Therefore, we can assume that simulations at neutral- and low-pH conditions are equilibrated. The average values from the two initial configurations for neutral and low pH will be used as references.
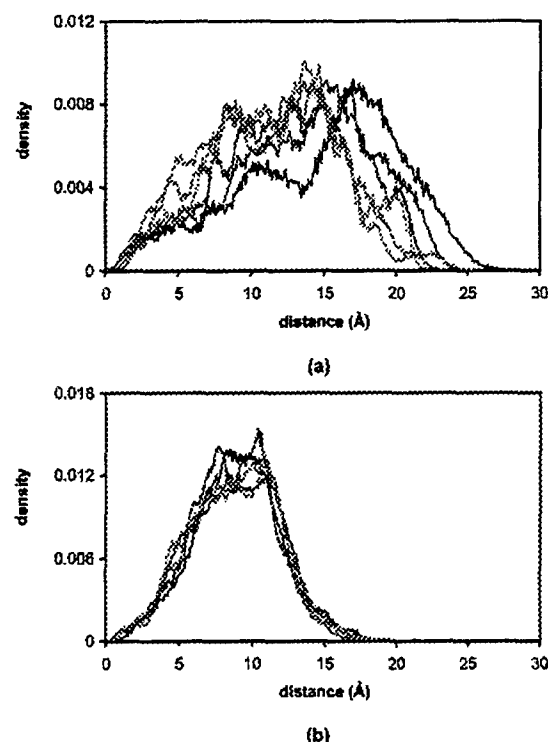
**Figure 5.** Atom densities of G2 dendrimer with water molecules at high pH as time progresses. Each graph consists of 300–500 ensembles. Simulation results at 0.3 ns (blue), 0.6 ns (purple), 0.9 ns (green), 1.2 ns (orange), 1.5 ns (red), and 1.8 ns (pink) from (a) ICN1 and (b) ICN2.

**Table 2. $R_G$ of PAMAM Dendrimer Generation 2**

| water | $r_c$ | $D$ | pH | $R_G$ (Å) |
|---|---|---|---|---|
| yes | ∞ | 1 | low | 18.87 ± 0.11[a] |
| | | | neutral | 16.47 ± 0.61[a] |
| | | | high | 13.28 ± 0.12, 9.47 ± 0.14[b] |
| no | 11 Å | 1 | low | 16.35 ± 0.11 |
| | | | neutral | 14.03 ± 0.05 |
| | | | high | 9.26 ± 0.14 |
| no | ∞ | 1 | low | 20.06 ± 0.09 |
| | | | neutral | 17.44 ± 0.11 |
| | | | high | 9.16 ± 0.18 |
| no | 11 Å | $r$ | low | 15.30 ± 0.18 |
| | | | neutral | 13.05 ± 0.21 |
| | | | high | 8.28 ± 0.07 |
| no | ∞ | $r$ | low | 16.59 ± 0.13 |
| | | | neutral | 14.47 ± 0.34 |
| | | | high | 8.43 ± 0.10 |

[a] Average value between results from ICN1 and ICN2. [b] Each value represents results from ICN1 and ICN2, respectively.

in our model is to shield charges because of its high dipole moment. We changed the vacuum dielectric constant ($D = 1$) to the distant-dependent dielectric constant ($D = r$) and compared the results with the data from simulations with water.

The radius of gyration $R_G$ of all G2 dendrimer models was calculated as

$$R_G = \sqrt{\frac{\sum m_i r_i^2}{\sum m_i}} \qquad (2)$$

and is presented in Table 2. All models show the same trends in pH dependency; with lower pH, $R_G$ increases. The difference between high and neutral pH is larger than between neutral and low pH. At neutral and low pH, $R_G$ of the $D = 1$, $r_c = 11$ Å model is similar to the $D = r$, $r_c = \infty$ model, the latter being slightly larger. Simulations with water molecules have the same long-range parameters of the $D = 1$, $r_c = \infty$ model. Including explicit water reduced the size of $R_G$. At high pH, $D = 1$ models show values closer to the simulation results of hydrated models than $D = r$ models.

Figures 6, 7, and 8 show the atom densities and the densities of terminal nitrogen atoms in G2 dendrimers without water molecules, compared to the results of simulation with water at high, neutral, and low pH. For relative comparisons between the total atom and the terminal nitrogen atom densities, the densities of terminal nitrogen atoms were normalized by the total atom numbers of their models, and the density values of terminal nitrogen atoms were increased to 3 times their real values for illustrative purposes. Since the terminal amines are reaction sites, special attention should be paid to the distribution of terminal nitrogen density in relation to the total atom density profile.

Figure 6 shows the density profile from simulations at high pH. Simulations from ICN1 (Figure 6e) have a radius more similar to all the nonhydrated models than to the simulations from ICN2 (Figure 6f). The atom density profile of the ICN1 model parallels the increase of the $D = 1$, $r_c = \infty$ model up to approximately 8 Å and then from 12.5 Å decreases closely with that of the $D = 1$, $r_c = 11$ Å model (Figure 6g). The atom density profile from the ICN2 model increases closely with that of the $D = r$ models up to 5 Å but then diverges from the other models. None of models without water show a peak shape of the atom density plot similar to the ICN1 or ICN2 models. The density profiles of the terminal
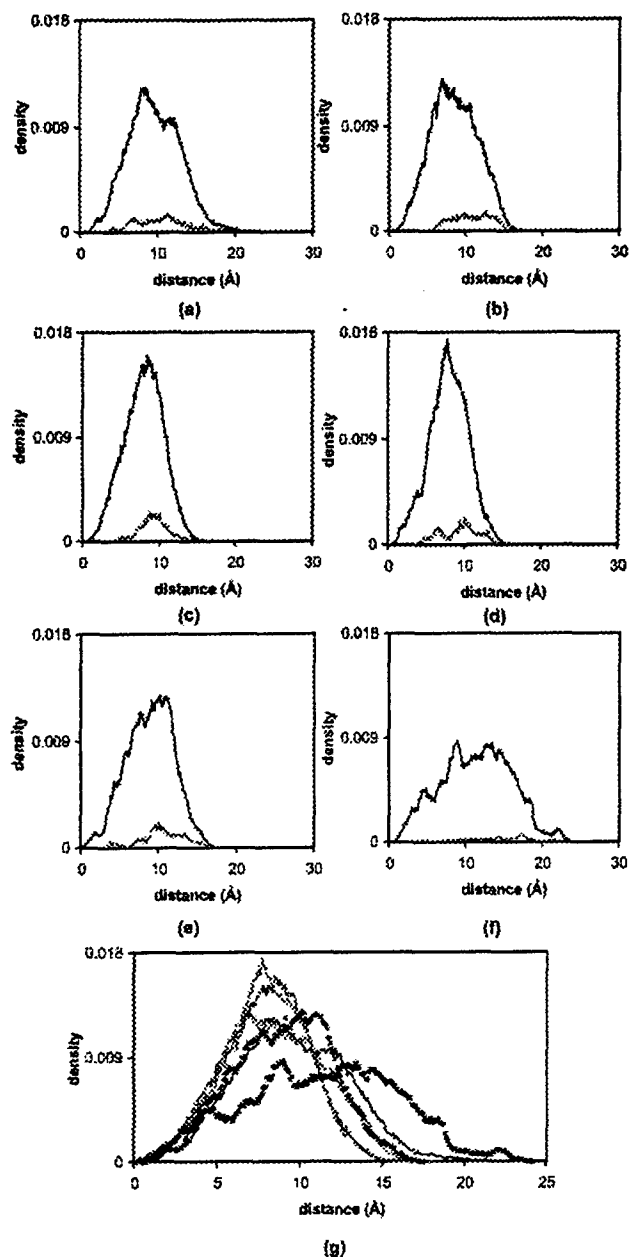
At high pH, however, density profiles from ICN2 are more compact than density profiles from ICN1 (Figure 3a,b). Moreover, the general shapes of the profiles are different from each other. Since the total charge of high pH models is zero, the hydrogen bond energy (included in Coulomb energy term in eq 1) and the Lennard-Jones energy are dominant among the nonbonded potential terms in eq 1. Figure 4 shows the hydrogen bond interaction between G2 dendrimer and water molecules after 200 ps simulation from ICN1 at high pH. This is just before the simulation at 1000 K for the preparation of ICN2. During the simulation at 1000 K, hydrogen bonding between water molecules is disrupted, resulting in the water being dispersed into vacuum space. During this brief removal of water the major energy contribution comes from van der Waals attraction so that some portions of the dendrimer chains are able to rearrange. Therefore, ICN2 is compact, while ICN1 is extended.

We tracked the simulation progress of hydrated G2 dendrimer at high pH. Figure 5 represents the atom densities of G2 dendrimer from ICN1 and ICN2 at progressing time intervals. Each plot consists of 300–500 ensembles. The ICN2 plots stay within a confined radial distance range, indicating a local minimum from which the system does not escape within the simulation time. The ICN1 plots move to the left on the distance axis as time progresses and generally settle into a different local minimum except in the outer tail portion. We will use the results from both ICN1 and ICN2 for the high-pH case, understanding their differences within our simulation limitations.

Nonhydrated G2 dendrimers were simulated under several long-range interaction conditions. The effect of nonbond cutoff distance $r_c$ was of major interest. Simulations with $r_c = 11$ Å and $r_c = \infty$ were compared. We also hypothesized that the most important role of water

**Figure 6.** Atom densities (blue) and the densities of terminal nitrogen atoms (red) in G2 dendrimers at high pH. The nonbonded interaction conditions of models without explicit water molecules are (a) $D = 1$ and $r_c = 11$ Å, (b) $D = 1$ and $r_c = \infty$, (c) $D = r$ and $r_c = 11$ Å, and (d) $D = r$ and $r_c = \infty$. They are compared with the results of simulation with water from (e) ICN1 and (f) ICN2. To improve the visual comparison, all density profiles of terminal nitrogen atoms are increased to 3 times their real value. The atom densities of all models are compared in (g): $D = 1$ and $r_c = 11$ Å (blue line), $D = 1$ and $r_c = \infty$ (pink line), $D = r$ and $r_c = 11$ Å (green line), $D = r$ and $r_c = \infty$ (red line), ICN1 (purple circle), and ICN2 model (brown circle).

nitrogen atoms present several notable features. The ICN1 model has several peaks. The $D = 1$, $r_c = 11$ Å and $D = 1$, $r_c = \infty$ models (Figure 6a,d) show similar peak distribution. Based on these density profiles, the distribution range of the ICN1 model is between the $D = 1$, $r_c = 11$ Å model and the $D = 1$, $r_c = \infty$ model. None of the nonhydrated models can reproduce the ICN2 model, while the $D = 1$, $r_c = 11$ Å model is the closest mimic of the ICN2 model.

The density profiles of simulations at neutral pH are presented in Figure 7. From the $D = 1$, $r_c = \infty$ model
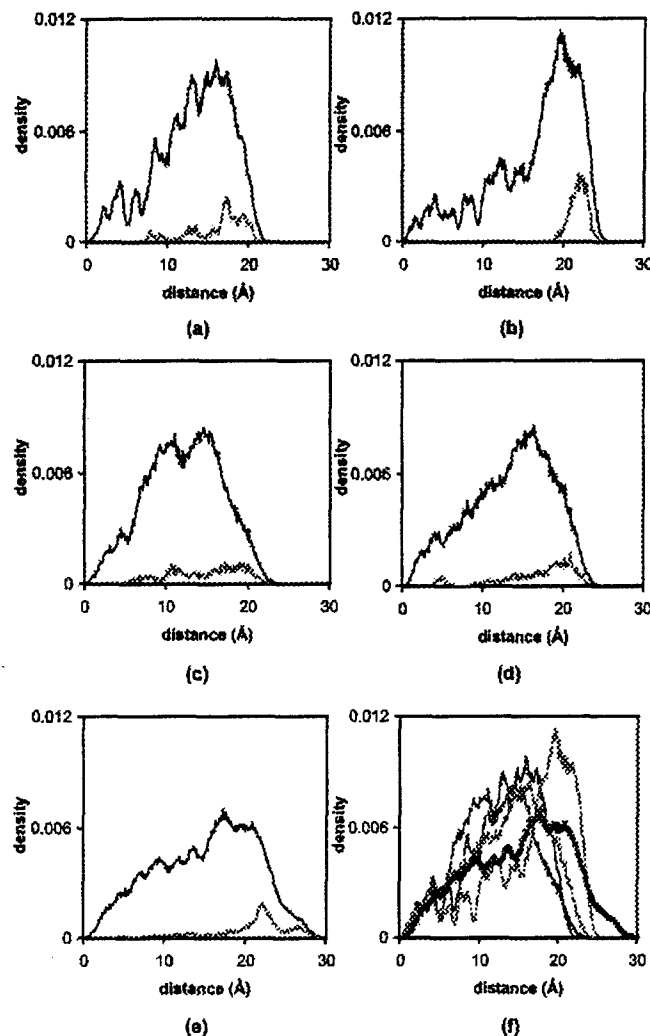


**Figure 7.** Atom densities (blue) and the densities of terminal nitrogen atoms (red) in G2 dendrimers at neutral pH. The nonbonded interaction conditions of models without explicit water molecules are (a) $D = 1$ and $r_c = 11$ Å, (b) $D = 1$ and $r_c = \infty$, (c) $D = r$ and $r_c = 11$ Å, and (d) $D = r$ and $r_c = \infty$. They are compared with (e) the results of simulation with water, which are the average values of results from ICN1 and ICN2. To improve the visual comparison, all density profiles of terminal nitrogen atoms are increased to 3 times their real value. The atom densities of all models are compared in (f): $D = 1$ and $r_c = 11$ Å (blue line), $D = 1$ and $r_c = \infty$ (pink line), $D = r$ and $r_c = 11$ Å (green line), $D = r$ and $r_c = \infty$ model (red line), and models with water molecules (purple circle).

(Figure 7b), a 10 Å water layer changed the density distribution dramatically (Figure 7e). The atom density distribution (blue) is expanded to a greater radius, and the density of terminal nitrogen atoms (red) spread down toward the center of mass. An additional outside tail bump also appeared, which is not present in any of the nonhydrated models. The atom density profile of the with-water model increased closely with the $D = r$, $r_c = \infty$ model up to ~ 12 Å and then spread out to larger radius (Figure 7f). Nevertheless, except in the tail region of the hydrated model, the shapes of the two models are similar. Additionally, some terminal nitrogen atoms of the $D = r$, $r_c = \infty$ model begin close to the center of mass and a main peak of the density profile of terminal nitrogen arises close to the outer part of the model (Figure 7d), which presents a very similar profile to results from the hydrated model (Figure 7e).

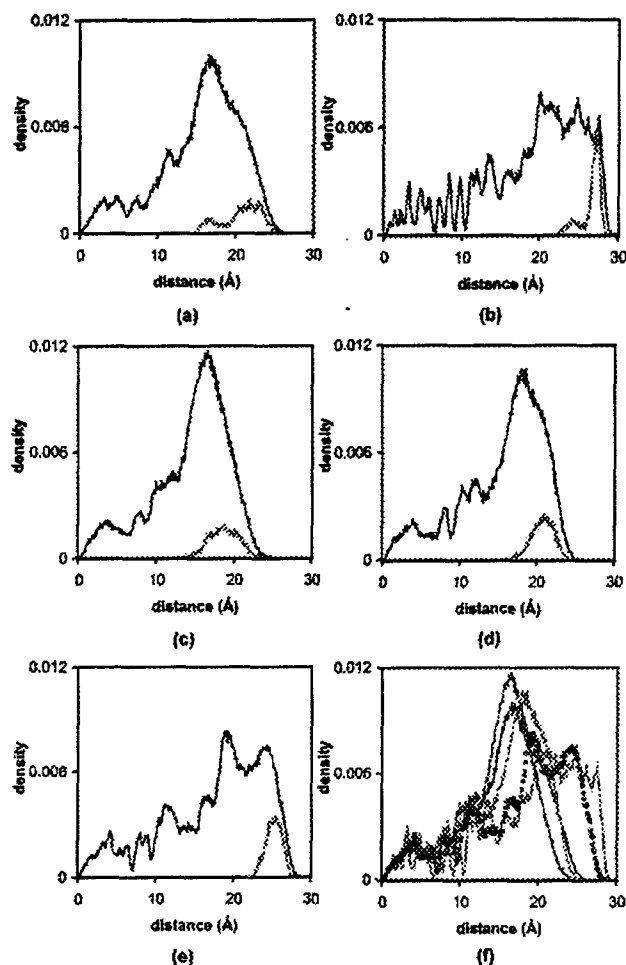Figure 8 shows the density profile of simulations at low pH. With the addition of a10 Å hydration layer,

**Figure 8.** Atom densities (blue) and the densities of terminal nitrogen atoms (red) in G2 dendrimers at low pH. The nonbonded interaction conditions of models without explicit water molecules are (a) $D = 1$ and $r_c = 11$ Å, (b) $D = 1$ and $r_c = \infty$, (c) $D = r$ and $r_c = 11$ Å, and (d) $D = r$ and $r_c = \infty$. They are compared with (e) the results of simulation with water, which are the average values of results from ICN1 and ICN2. To improve the visual comparison, all density profiles of terminal nitrogen atoms are increased to 3 times their real value. The atom densities of all models are compared in (f): $D = 1$ and $r_c = 11$ Å (blue line), $D = 1$ and $r_c = \infty$ (pink line), $D = r$ and $r_c = 11$ Å (green line), $D = r$ and $r_c = \infty$ model (red line), and models with water molecules (purple circle).

some shrinking of the radial distance from the $D = 1$, $r_c = \infty$ model is observed (Figure 8f). The atom density profiles of all models increase similarly up to 12 Å. After 12 Å, the density profile of the hydrated model lies in between the $D = r$, $r_c = \infty$ model and the $D = 1$, $r_c = \infty$ model, though closer to the latter. The largest 4 Å region of atom density profiles of the $D = r$, $r_c = \infty$ model and hydrated model are, however, very similar. Interestingly, the two-peak profile of the terminal nitrogen density of the $D = 1$ models (Figure 8a,b) disappears in Figure 8e, which is the also the case of the $D = r$ models (Figure 8c,d). The terminal nitrogen distribution of all the atoms of the $D = r$, $r_c = \infty$ model is closest to that of the hydrated model, only slightly broadened.

From Table 2 and Figures 6−8, the best condition to mimic simulations with water within the limitation of our hydration model is $D = r$, $r_c = \infty$ at neutral and low pH and $D = 1$, $r_c = 11$ Å at high pH. Still, the $D = r$, $r_c = \infty$ model at high pH is reasonable if we keep in mind that the overall structure is more condensed (a narrower and left-shifted profile in the atom density distribution)

than the ICN1 model. The atom density profile of the $D = r$, $r_c = \infty$ model is narrower, but the density profile of terminal nitrogen is very close to corresponding results from simulation with water. In particular, the terminal groups, which would be essential for chemical and biological functionality, show similar behavior which validates the use of waterless simulation for the current purpose. Therefore, we will use PAMAM dendrimer simulations including all long-range interactions with distance-dependent dielectric constant as a substitute for the explicit water simulation for the remainder of this paper.

We studied the PAMAM dendrimer configuration as a function of pH and dendrimer generation. The final configurations of PAMAM dendrimer generation 6, after 100 ps of MD simulation, at different pH conditions, are shown in Figure 9. The final configuration of dendrimer at high pH is globular and loosely compact (Figure 9a). From the previous simulation results and discussion, we know the overall shape is probably more compressed than simulations with water molecules. With the protonation of the primary amines at neutral pH, the dendrimer configuration is more bulky, bearing large internal cargo spaces due to electrostatic repulsion (Figure 9b). The final configuration at low pH presents a highly ordered structure with extensively stretched dendrimer branches, generally producing an open structure (Figure 9c). These conformational changes by pH can be applied to the drug-loading scheme in the dendrimer. Analytic comparison is done by the atom density distribution and the density of terminal nitrogen atoms as shown in parts a and b of Figure 10, respectively. As pH changed from high to low pH, the interior atom density is reduced, yielding additional interior space. There is no significant initial configuration dependency of the ICN1 (blue) and ICN2 (red) model (Figure 10).

Dendrimer conformation change was investigated as a function of generation number. Atom density and the density of terminal nitrogen atoms of the PAMAM dendrimer as a function of dendrimer generation at high, neutral, and low pH are presented in Figure 11. The atom density is normalized by total atom number of G6 dendrimer, and the density of terminal nitrogen atoms is normalized by the total number of terminal nitrogen atoms of G6 dendrimer at each pH condition. As the generation increases, the density profile moves to larger radial distance from the center of mass. Table 3 presents maximum radius $r_{max}$ and maximum density radius $r_d$ of all these graphs, in addition to $R_G$ values for all models.

Figure 11a shows atom density profile over radial distance from center of mass of generation-$n$ dendrimer at high pH. The density graph of generation $n$ is stacking up on that of generation $n − 1$. Generation $n − 1$ parts are conserved, adding the additional density in the outer radial region. This means the atom distribution at high pH is stable, showing that the dendrimer at high pH preserves compact structure as far as branch stiffness permits. In the region of $r > r_d$, $|\partial \rho/\partial r|$ (asymptotic value) sharply increases from generation 4. Since the density profile is radial, only the profile at $r > r_d$ can be compared as polymer brush[28] analogy. Our graphs present similar dropping shape with the results from coarse-grain MD simulations of grafted polymer brush:[29] (1) generations 2 and 3: low surface density; (2) generations 4, 5, and 6: high surface density.
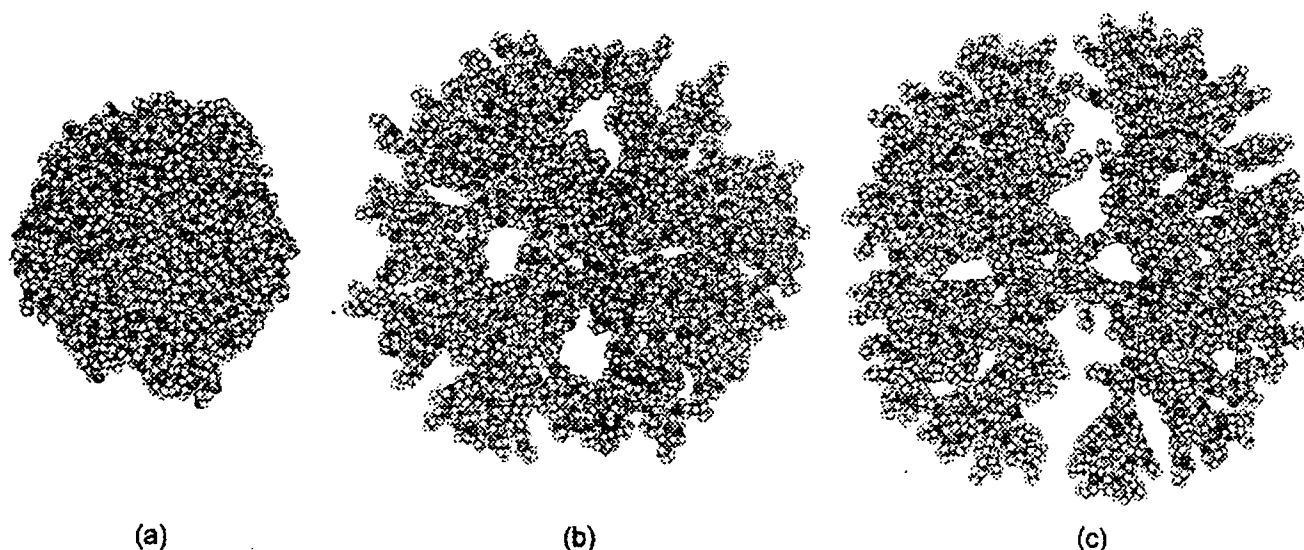
**Figure 9.** Final configuration of G6 PAMAM dendrimer after 100 ps MD simulations (a) at high pH (no amine is protonated), (b) at neutral pH (primary amines are protonated), and (c) at low pH (all amines are protonated).
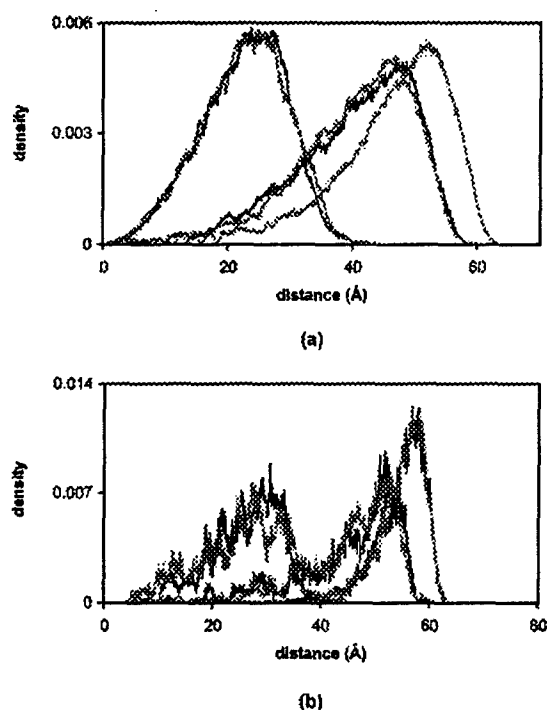


**Figure 10.** (a) Total atom density and (b) the density of terminal nitrogen atoms of G6 PAMAM dendrimer at different pH conditions from ICN1 (blue line) and ICN2 (red line). As pH decreases, the density profile moves to a larger radial distance from the center of mass.

However, $|\partial\rho/\partial r|$ at $r > r_{\mathrm{d}}$ (except for the tail region) of G4 dendrimer in Figure 11b (the density profile of terminal nitrogen atoms) is between those of the G2 and G3 dendrimers and those of the G5 and G6 dendrimers. Therefore, dendrimers higher than generation 5 seem to demonstrate a dense-packing structure relative to the intermediate G4 dendrimer. Interestingly, the terminal nitrogen density graph of generation $n$ also presents stacking up feature on that of generation $n - 1$. This means a longer branched chain end has the same probability of being in the inner region of the dendrimer. The branched dendrimer chains should be flexible enough for this back-folding to occur. The mean shift of $r_{\mathrm{d}}$ from atom density profile to terminal nitrogen density

one for all generations is about 123% at high pH. These shifts do not show generation dependency.

The density profile at neutral pH shows a different generation dependency as shown in Figure 11c,d. The atom density of generation-$n$ dendrimer is higher than that of generation $n - 1$, in the region around $r_{\mathrm{d}}$ of generation $n - 1$. Higher generation dendrimers provide a denser intermediate region with a sparse interior. If a dendrimer is used for drug loading, it may be difficult to put the drug cargo into the interior of higher generation dendrimer at neutral pH, but it could be a good carrier once drugs are loaded. The density of terminal nitrogen atoms appears at broad radial range for each generation at neutral pH. This implies that significant branch back-folding occurred at neutral pH, in addition to the major peripheral distribution of the terminal groups. The density profiles of terminal nitrogen atoms show multiple local peaks for all generations. There seems to be preferential radii for branched terminal atoms to locate. $|\partial\rho/\partial r|$ at $r > r_{\mathrm{d}}$ increases gradually as generation grows in both total atom and terminal nitrogen atom density profiles. The mean shift of $r_{\mathrm{d}}$ from atom density profile to terminal nitrogen density one is about 114% at neutral pH.

Contrary to the neutral pH case, the atom density profile of generation-$n$ dendrimer at low pH (Figure 11e) is lower than that of generation $n - 1$, in the whole region of generation $n - 1$. As generation increases, the dendrimer molecule becomes less dense in the interior and extends out from the center of mass. Therefore, higher generation dendrimer at low pH may be the best to diffuse in and out small noncharged molecules such as drugs. $|\partial\rho/\partial r|$ at $r > r_{\mathrm{d}}$ increases evenly as generation grows in atom density profiles. The density profiles of terminal nitrogen atoms are localized on the periphery of dendrimer molecules as shown in Figure 11f. At low pH, protonated inner amines prevent the protonated terminal amines from folding back into the inside of the dendrimer, leaving terminal amines on the periphery of the dendrimer. The minimum radii $r_{\mathrm{min}}$ for nonzero terminal density are 16, 19.9, 25.9, 17, and 25.4 Å for generations 2 to 6, respectively. The ratios of $(r_{\mathrm{d}} - r_{\mathrm{min}})/(r_{\mathrm{max}} - r_{\mathrm{d}})$ at generations 2–6 are 1.2, 1.8, 1.6, 4.3, and 4.2. These kinds of G5 and G6 dendrimer graphs are reminiscent of the free end probability graphs
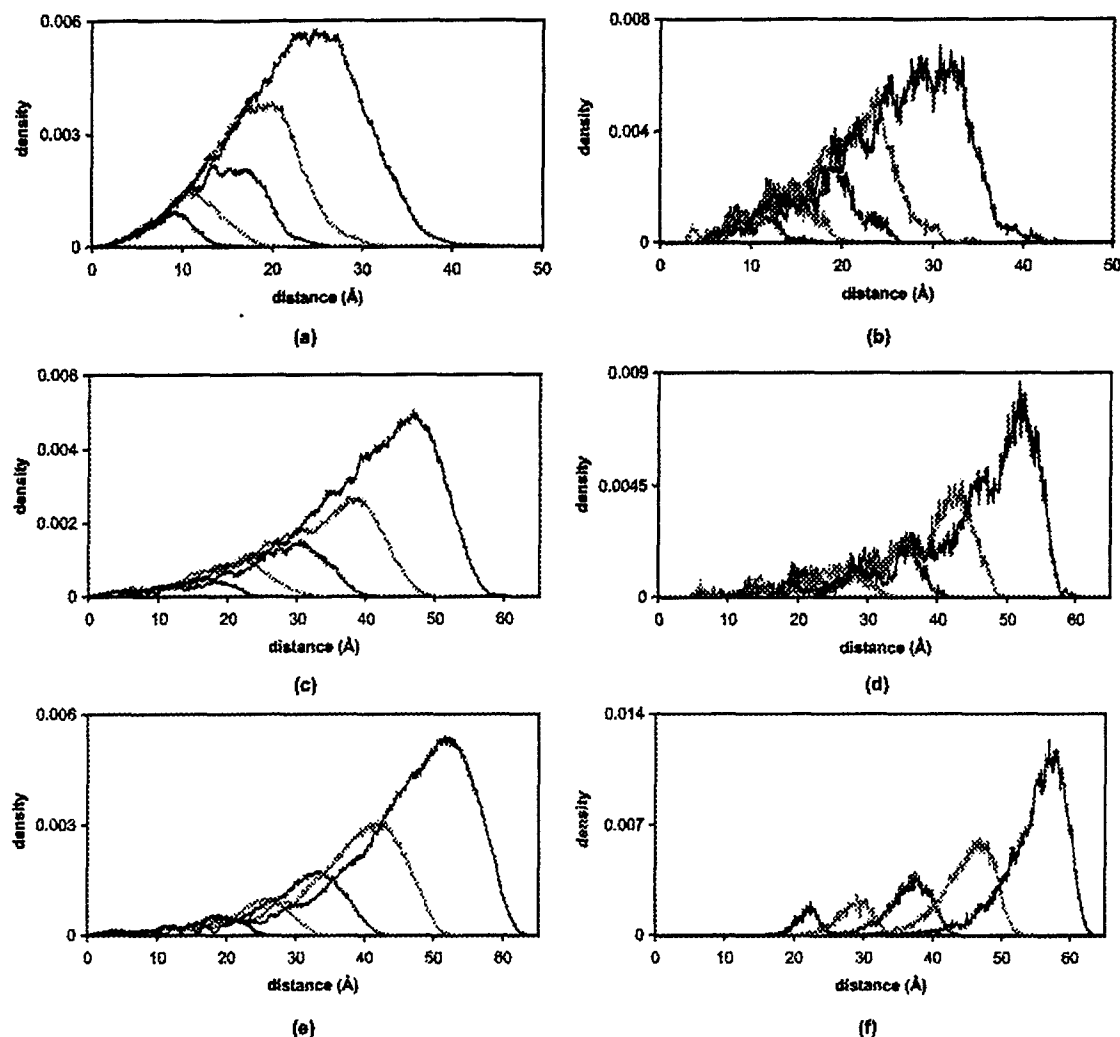
**Figure 11.** Density profile of the PAMAM dendrimer at high pH (a, b), neutral pH (c, d), and low pH (e, f) as a function of dendrimer generation: generation 2 (black), 3 (pink), 4 (green), 5 (red), and 6 (blue). The atom densities (left panel: a, c, e) are normalized by total atom number of G6 dendrimer and the densities of terminal nitrogen atoms (right panel: b, d, f) are normalized by the number of total terminal nitrogen atoms of G6 dendrimer at each pH. As the generation increases, the density profile moves to a larger radial distance from the center of mass.

**Table 3. Maximum Radius $r_{max}$ and Maximum Density Radius $r_d$ of Figure 11, in Addition to $R_G$ Values for All Models**

| generation | pH | $r_{max}$ (Å) | $r_d$ (Å) atom density | $r_d$ (Å) density of terminal N | $R_G$ (Å) |
|---|---|---|---|---|---|
| 2 | low | 27.7 | 19.2 | 22.4 | $16.6 \pm 0.1$ |
|   | neutral | 25.3 | 17.0 | 19.6 | $14.5 \pm 0.3$ |
|   | high | 19 | 9.3 | 10.5 | $8.4 \pm 0.1$ |
| 3 | low | 35.8 | 26.3 | 30.1 | $22.8 \pm 0.2$ |
|   | neutral | 34.6 | 22.7 | 27.8 | $19.7 \pm 0.1$ |
|   | high | 21.6 | 11.2 | 14.3 | $11.6 \pm 0.2$ |
| 4 | low | 44.7 | 33.9 | 37.6 | $29.9 \pm 0.1$ |
|   | neutral | 42.7 | 31.0 | 36.0 | $26.7 \pm 0.2$ |
|   | high | 27.4 | 15.3 | 19.2 | $14.8 \pm 0.1$ |
| 5 | low | 54.1 | 42.3 | 47.1 | $38.0 \pm 0.1$ |
|   | neutral | 51.7 | 39.4 | 42.5 | $32.8 \pm 0.7$ |
|   | high | 32.8 | 19.5 | 24.0 | $18.3 \pm 0.3$ |
| 6 | low | 64.2 | 52.3 | 56.8 | $46.8 \pm 1.0$ |
|   | neutral | 61.8 | 47.3 | 51.8 | $41.3 \pm 0.1$ |
|   | high | 44.1 | 24.8 | 30.7 | $24.2 \pm 0.4$ |

obtained from coarse-grain MD simulation of polymer brush at higher surface densities.[29] $|\partial \rho / \partial r|$ at $r > r_d$ of terminal nitrogen density graphs increases gradually as generation grows except generations 2 and 3, and the mean shift of $r_d$ from atom density profile to terminal nitrogen density is about 112%.

A simple model for polymer brushes gives polymer height $h$ from free energy minimization such as[28]

$$h \sim N(w\sigma a^2)^{1/3} \qquad (3)$$

where $a$ is the Kuhn length, $N$ is length measured by $a$, $w$ is the excluded-volume parameter, and $\sigma$ is the surface grafting density. Our model of PAMAM dendrimer is spherical with branch functionality being two.[14] It is difficult to properly correlate a property with $\sigma$ for comparison purposes. However, $N$ can be relatively correlated to the value of generation $-$ 1. As shown in Figure 12a, EDA core part has roughly half of the branch length. If we ignore the EDA core, the radial difference between $n$ and $n - 1$ branch points can analogue to $a$ as shown in Figure 12b; then the radial distance $L$ measured by radial $a$ equals generation $-$ 1. From Table 3, we could obtain the $r_{max}$ and $L$ relation for each pH condition such as

$$r_{max} \propto L^{\alpha} \qquad (4)$$

The values of exponent $\alpha$ are 0.97, 1.04, and 0.99 at high, neutral, and low pH, respectively. Even though the dense packing seems to start from generation 5 at high and low pH on the basis of the shape of terminal
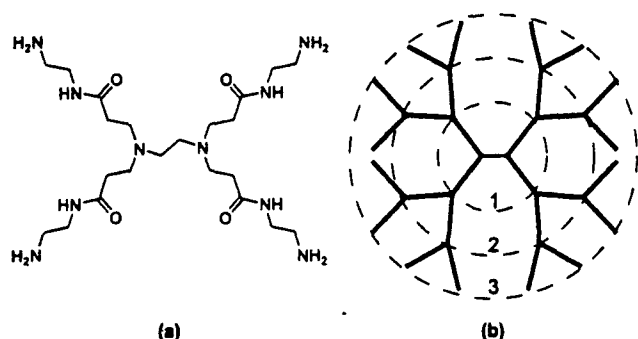
**Figure 12.** (a) Chemical structure of G0 PAMAM dendrimer with EDA core. (b) Schematic drawing of G2 PAMAM dendrimer where the circles represent central structure (a). Denoted numbers are the radial distance $L$ (= generation − 1).
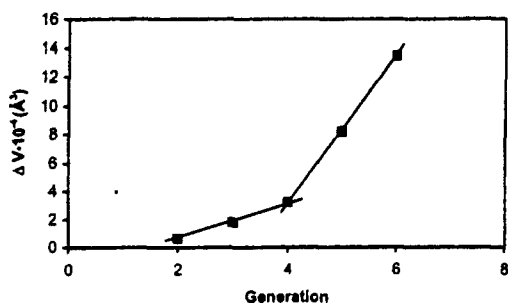


**Figure 13.** Volume change between neutral and low pH as a function of generation. Volumes were calculated as $R_G$ assuming a spherical dendrimer model. Lines are added to show linear regions.

nitrogen distribution and literature,[14] $r_{max}$ grows quickly as $L$ increases. On the other hand, total number of branch arms in a dendrimer can be defined as $N$ (28, 60, 124, 252, and 508 for G2 to G6 dendrimer, respectively). In this case, the exponents are 0.29, 0.30, and 0.29 at high, neutral, and low pH, respectively. Obviously, $r_{max}$ grows very slowly as $N$ increases, which gives the small, defined size of dendrimers, while the chain dimension $R_G$ of random-coiled polymer grows as $N^{1/2}$.

Previous gene delivery experiments found a good amount of gene expression from dendrimer generations greater than 5.[3] One characteristic of a dendrimer as a gene delivery vector is thought to be the ability to escape the endosomal compartment. This may result from further protonation of the dendrimer at endosomal pH 5, as compared to pH 7.4 outside the cell and in the cytosol, causing endosomal disruption due to volume change driven by osmotic forces.[30] The volume change between neutral and low pH is, therefore, of interest. Figure 13 represents the volume change between neutral and low pH at each generation. Volumes were calculated as $R_G$ assuming a spherical dendrimer model. A transition of volume change happens at generation 4. This feature was also observed from Figure 11b. There should be a distinct improvement in cytosolic delivery from generation 4 to 5. Therefore, we can account for the generation dependency of gene expression based on this endosomal disruption hypothesis.

**Conclusion**

Extensive MD simulations of G2 PAMAM dendrimer with explicit water molecules were performed from two different initial configurations over a range of pH conditions. The effects of long-range interaction parameters such as interaction distance and dielectric constant

were investigated in simulations of the same dendrimer models without water in order to find an optimal set of conditions for waterless simulation. After comparison of results for hydrated and nonhydrated G2 PAMAM dendrimers over a range of simulation parameter settings, we found the optimal condition was a distance-dependent dielectric constant without a nonbonded energy cutoff. The general simulation results of the G2 PAMAM dendrimers with these parameters corroborate the simulations done with 10 Å explicit water layers, especially in the charged dendrimer models at neutral and low pH. At high pH, the overall conformation is a slightly compressed under these long-range interaction conditions compared to the hydrated model.

PAMAM dendrimers of generations 3−6 were continuously simulated using optimal parameter settings for waterless simulation over a range of pH conditions. The radial atom density of each dendrimer was determined for each pH value. Globular and loosely compact structures for generation-$n$ dendrimer at high pH ($\geq 10$) showed a radial atom density profile which conserves the generation $n − 1$ interior while adding the additional outer layer. Highly ordered extended generation-$n$ dendrimer structures at low pH ($\leq 4$) produce an atom density profile that is reduced in the region corresponding to generation $n − 1$. This hollowing of the interior as generation increases, within our simulation range, can provide increased access to the interior by other chemical agents. By contrast, significant branch back-folding occurring at neutral pH, in addition to the major peripheral distribution of the terminal groups, yields an atom density profile of generation-$n$ dendrimer that is higher in the region around the maximum density of the generation $n − 1$. This suggests that the higher generation dendrimer provide a cavity surrounded by dense atom populations, which should be a more stable agent carrier. The volume differences between neutral and low pH calculated from $R_G$ showed a significant increase beginning with generation 5. These structural differences are possibly responsible for the improvement in gene expression at G5 dendrimer as a gene delivery system.

**References and Notes**

(1) Eldridge, J. H.; Staas, J. K.; Meulbroek, J. A.; Tice, T. R.; Gilley, R. M. *Infect. Immun.* **1991**, *59*, 2978−2986.
(2) Kukowska-Latallo, J. F.; Bielinska, A. U.; Johnson, J.; Spindler, R.; Tomalia, D. A.; Baker Jr., J. R. *Proc. Natl. Acad. Sci. U.S.A.* **1996**, *93*, 4897−4902.
(3) Haensler, J.; Szoka, Jr., F. C. *Bioconjugate Chem.* **1993**, *4*, 372−379.
(4) Maruyama-Tabata, H.; Harada, Y.; Matsumura, T.; Satoh, E.; Cui, F.; Iwai, M.; Kita, M.; Hibi, S.; Imanishi, J.; Sawada, T.; Mazda, O. *Gene Ther.* **2000**, *7*, 53−60.
(5) Malik, N.; Evagorou, E. G.; Duncan, R. *Anti-Cancer Drugs* **1999**, *10*, 767−776.
(6) Thompson, J. P.; Schengrund, C. L. *Glycoconjugate J.* **1997**, *14*, 837−845.
(7) Wyman, T. B.; Nicol, F.; Zelphati, O.; Scaria, P. V.; Plank, C.; Szoka, Jr., F. C. *Biochemistry* **1997**, *36*, 3008−3017.

(8) van Duijvenbode, R. C.; Borkovec, M.; Koper, G. J. M. *Polymer* **1998**, *39*, 2657–2664.

(9) Boris, D.; Rubinstein, M. *Macromolecules* **1996**, *29*, 7251–7260.

(10) Mansfield, M. L.; Klushin, L. I. *Macromolecules* **1993**, *26*, 4262–4268.

(11) Cai, C.; Chen, Z. Y. *Macromolecules* **1997**, *30*, 5104–5117.

(12) Naylor, A. M.; Goddard III, W. A.; Kiefer, G. E.; Tomalia, D. A. *J. Am. Chem. Soc.* **1989**, *111*, 2339–2341.

(13) Murat, M.; Grest, G. S. *Macromolecules* **1996**, *29*, 1278–1285.

(14) Tomalia, D. A.; Naylor, A. M.; Goddard III, W. A. *Angew. Chem., Int. Ed. Engl.* **1990**, *29*, 138–175.

(15) Morgenroth, F.; Kubel, C.; Mullen, K. *J. Mater. Chem.* **1997**,

(20) Gorman, C. B.; Smith, J. C. *Polymer* **2000**, *41*, 675–683.

(21) Cagin, T.; Wang, G.; Martin, R.; Breen, N.; Goddard III, W. A. *Nanotechnology* **2000**, *11*, 77–84.

(22) Welch, P.; Muthukumar, M. *Macromolecules* **1998**, *31*, 5892–5897.

(23) Nisato, G.; Ivkov, R.; Amis, E. J. *Macromolecules* **2000**, *33*, 4172–4176.

(24) Chen, W.; Tomalia, D. A.; Thomas, J. L. *Macromolecules* **2000**, *33*, 9169–9172.

(25) Simonson, T.; Archontis, G.; Karplus, M. *J. Phys. Chem. B* **1999**, *103*, 6142–6156.

(26) Lifson, S.; Hagler, A. T.; Dauber, P. *J. Am. Chem. Soc.* **1979**, *101*, 5111–5121.